UDC 535.37
IRSTI 29.19.22

https://doi.org/10.55452/1998-6688-2026-23-3-473-485

[1]Tulegenova A.T.,
associate professor, PhD, ORCID ID: 0000-0002-5701-6674,
e-mail: tulegenova.aida@gmail.com
[2]Lisitsyn V.M.,
professor, Dr.Sci., ORCID ID: 0000-0002-2075-4796,
e-mail: lisitsyn@tpu.ru
[1]Nogaibekova G.Zh.,
senior lecturer, ORCID ID: 0009-0008-8688-4279,
e-mail: nogaibekovagulnur@gmail.com
[3]Lisitsyna L.A.,
professor, Dr.Sci., ORCID ID: 0000-0001-6273-6345,
e-mail: lisitsyna@mail.ru

[1]Al-Farabi Kazakh National University, Almaty, Kazakhstan
[2]Tomsk Polytechnic University, Tomsk, Russia,
[3]Tomsk State University of Architecture and Building, Tomsk, Russia

INFLUENCE OF THE AL/GA RATIO ON THE OPTICAL PROPERTIES OF $Y_3AL_XGA_{5-X}O_{12}$:CE PHOSPHORS FOR LED APPLICATIONS

Abstract

This paper presents the results of studies on $Y_3Al_xGa_{5-x}O_{12}$: Ce (YAGG:Ce) ceramic phosphors synthesized for the first time using a radiation method. The influence of the Al/Ga ratio on the optical properties of Ce^{3+}-doped $Y_3Al_xGa_{5-x}O_{12}$: Ce (YAGG:Ce) garnet phosphors, which are promising for LED light source applications, was investigated. Excitation and photoluminescence spectra of samples with different aluminum and gallium contents at a fixed concentration of Ce^{3+} activator ions were analyzed. It was shown that variations in composition lead to changes in the position and shape of the excitation and emission bands, variations in the photoluminescence band width, as well as redistribution of the emission intensity under excitation in the ultraviolet and blue spectral regions. It was found that a decrease in the Al/Ga ratio causes the excitation band to shift toward the longer wavelength region near 340–370 nm, which increases the excitation efficiency when near-ultraviolet and violet LEDs are used. The obtained results confirm the feasibility of using the radiation method for the synthesis of efficient YAGG:Ce phosphors.

Keywords: phosphors, $Y_3Al_xGa_{5-x}O_{12}$:Ce, Al/Ga ratio, excitation spectra, photoluminescence, LEDs, ultraviolet.

Received April 4, 2026; revised August 20, 2026; accepted August 26, 2026.

Introduction

Cerium (III)-activated garnet phosphors constitute the most technologically mature class of inorganic luminescent materials for solid-state lighting, combining exceptional thermal stability, chemical inertness, and a broadband visible emission that affords efficient conversion of blue or near-ultraviolet (n-UV) pump radiation into white light [1]. The archetype, $Y_3Al_5O_{12}$:Ce (YAG:Ce), remains the dominant phosphor in commercial white LEDs based on InGaN blue chips [2]. The rapid proliferation of high-power laser-driven phosphor converters (LPCs) and remote-phosphor configurations, however, imposes demanding additional requirements: elevated saturation thresholds, superior thermal quenching resistance, and narrowly tailored emission spectra for precision colorimetry [3,4].

Contemporary phosphor engineering for solid-state lighting increasingly demands spectral tunability – the capacity to independently optimize excitation and emission profiles for diverse pump sources and target colour-rendering specifications [5]. Partial or complete isovalent substitution of Al^{3+} by the larger Ga^{3+} (ionic radius in octahedral coordination: $r(Al^{3+}) = 0.535$ Å vs. $r(Ga^{3+}) = 0.620$ Å) in the $Y_3(Al,Ga)_5O_{12}$:Ce matrix expands the unit-cell volume, modifies the crystal-field splitting of the 5d levels of Ce^{3+}, and produces systematic red-shifts of both excitation and emission bands [6,7]. Such compositional flexibility has been exploited for a wide range of garnet systems, yet rigorous, composition-by-composition investigations covering the full $Y_3Al_xGa_{5-x}O_{12}$: Ce series ($0 \leq x \leq 5$) remain limited in the literature.

A central practical consideration is the excitation wavelength. The majority of commercial white LEDs exploit 450–465 nm InGaN chips, yet a growing segment of high-CRI and horticultural applications employs n-UV/violet sources (380–410 nm), for which efficient UV-band excitation is critical [8]. In Ce^{3+}-doped garnets, two distinct 4f → 5d absorption manifolds are observable: a higher-energy band near 340–370 nm (4f → $5d^2$) and a lower-energy band near 430–470 nm (4f → $5d^1$); compositional modification redistributes oscillator strength between these manifolds, thereby altering the efficacy under different pump wavelengths [9]. Conversion efficiency is additionally governed by the structural perfection of the luminescence centers, which is in turn sensitive to synthetic conditions. High-temperature solid-state reactions and solution-combustion routes are capable of producing phase-pure ceramics, but their multi-hour processing cycles constrain compositional screening and optimization.

Direct electron-beam radiation synthesis–first demonstrated for garnet ceramics in 2017-offers an attractive alternative: phase-pure ceramics are produced in sub-second irradiation times (≤ 1 s) from stoichiometric oxide mixtures, without any mineralizer additives and at throughputs reaching ≈5 g s−1[10]. The present work extends this synthesis platform to the multi-component $Y_3Al_xGa_{5-x}O_{12}$: Ce system and provides a comprehensive characterization of structural, spectral, luminance, and colour properties as a function of Al/Ga composition, benchmarked against literature data for thermally synthesized counterparts.

Materials and methods

Ceramic synthesis. Ceramic phosphors were fabricated by direct high-energy electron-beam irradiation of stoichiometric oxide precursor mixtures. Irradiation was performed on an ELV-6 electron accelerator at the Budker Institute of Nuclear Physics (SB RAS, Novosibirsk, Russia) at a beam energy of 1.4 MeV and a power density in the range 1–30 kW cm^{-2}.

Precursor preparation. Powder mixtures of Y_2O_3, Al_2O_3, and Ga_2O_3 were prepared in stoichiometric ratios corresponding to the target garnet formula $Y_3Al_xGa_{5-x}O_{12}$: Ce. Ce_2O_3 was added as activator at 0.5 wt.% relative to the total charge mass. All precursor oxides were supplied by Hebei Suoyi New Material Technology Co., Ltd. (grades K1, K6, K7, K8), with a purity ≥99.95% and comparable particle-size distributions, ensuring consistency of synthesis conditions across the composition series. Sample designations follow the internal numbering adopted by the authors.

Irradiation geometry. The charge was loaded into a massive copper crucible (inner dimensions 10 × 5 × 1 cm^3, depth 10 mm), which served simultaneously as the reaction vessel and heat sink. A 1 cm^2 electron beam scanned transversally at 50 Hz while the crucible was translated at 1 cm s^{-1} relative to the scanning beam, ensuring uniform energy deposition over the entire charge area. At the crucible depth employed, the electron range did not reach the copper bottom, precluding contamination of the charge by copper. Following irradiation, the ceramics were cooled, extracted from the crucible, and recovered as dense plates (Figure 1). For spectroscopic characterization, the ceramic plates were mechanically comminuted into powder, eliminating surface-geometry artefacts inherent in measurements on bulk ceramic specimens.

Synthesis yield. The synthesis yield η was defined as the ratio of the recovered ceramic mass to the initial charge mass, expressed as a percentage. The mass of the synthesized ceramic plates ranged

from approximately 45 to 60 g; the observed scatter is attributed to irreproducible compaction and levelling of the charge prior to irradiation. Notwithstanding this variability, the selection of starting materials and process parameters consistently afforded high synthesis yields of 90–97% (Table 1).

Table 1 – Nominal compositions of $Y_3Al_xGa_{5-x}O_{12}$:Ce ($0 \le x \le 5$) ceramics (series 636–641) and synthesis yields

Sample	Formula	Precursor charge composition (wt.%)	Yield, %
636	$Y_3Al_5O_{12}$:Ce	Al2O3 – 43; Y2O3 – 57; Ce2O3 – 0.5	96.5
637	$Y_3Al_4GaO_{12}$:Ce	Al2O3 – 32; Y2O3 – 53; Ga2O3 – 15; Ce2O3 – 0.5	96.3
638	$Y_3Al_3Ga_2O_{12}$:Ce	Al2O3– 22.5; Y2O3 – 50; Ga2O3 – 27.5; Ce2O3 – 0.5	96.3
639	$Y_3Al_2Ga_3O_{12}$:Ce	Al2O3 – 14; Y2O3 – 47; Ga2O3 – 39; Ce2O3 – 0.5	97.2
640	$Y_3AlGa_4O_{12}$:Ce	Al2O3 – 6.7; Y2O3 – 44.3; Ga2O3 – 49; Ce2O3 – 0.5	96.6
641	$Y_3Ga_5O_{12}$:Ce	Y2O3 – 42; Ga2O3 – 58; Ce2O3 – 0.5	94.4

Note: Precursor mixture compositions are normalized to 100 wt.% for the host oxide mixture (Y_2O_3 + Al_2O_3 ± Ga_2O_3); Ce_2O_3 (0.5 wt.%) is added as an activator in addition to the host, so each row totals 100.5 wt.%.

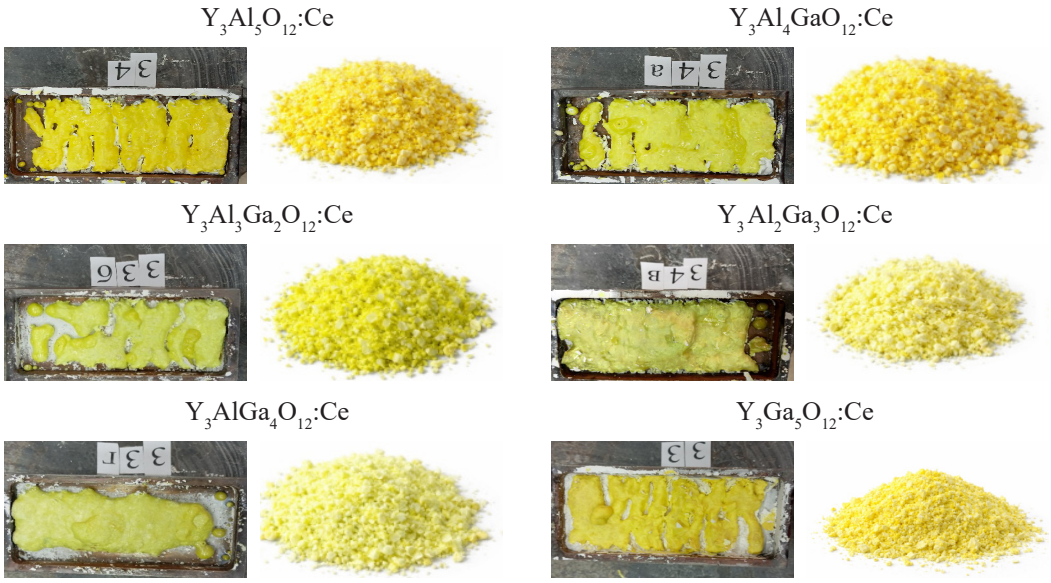

Figure 1 – Photographs of as-synthesized ceramic specimens in copper crucibles

X-ray diffraction. Phase composition and crystal structure were characterized by X-ray diffraction (XRD) using a Rigaku MiniFlex 600 diffractometer (Rigaku Corporation, Tokyo, Japan) with Cu Kα radiation (λ = 1.5406 Å), operated at 40 kV / 15 mA, over a 2θ range of 3–90° with a step size of 0.02°.

Photoluminescence and excitation spectroscopy. Photoluminescence (PL) emission and photoluminescence excitation (PLE) spectra were recorded on a Cary Eclipse fluorescence spectrophotometer (Agilent Technologies, USA), equipped with a xenon flash lamp source and a photomultiplier tube detector. Excitation and emission slit widths were set to 5 nm / 5 nm. All spectra were recorded at room temperature ~23 ± 2 °C on powdered specimens.

Diffuse reflectance spectroscopy. Diffuse reflectance spectra were recorded over the 200–600 nm range using a Cary series UV-Vis-NIR spectrophotometer (Agilent Technologies) equipped with an integrating sphere (DRA) accessory.

Relative luminance. Relative luminance was measured using a Konica Minolta LS-150 luminance meter (Konica Minolta, Tokyo, Japan) under fixed excitation and geometrical conditions (excitation wavelength, angle, and working distance identical for all specimens), referenced to the SDL-4000 phosphor standard measured under the same conditions.

Results and discussion

Crystal structure and phase composition

The crystal structure of the $Y_3Al_xGa_{5-x}O_{12}$:Ce ($0 \leq x \leq 5$) was characterised by X-ray powder diffraction (XRD). The diffractograms are presented in Figure 2a (full angular range) and Figure 2b (expanded region $2\theta = 20–40°$).

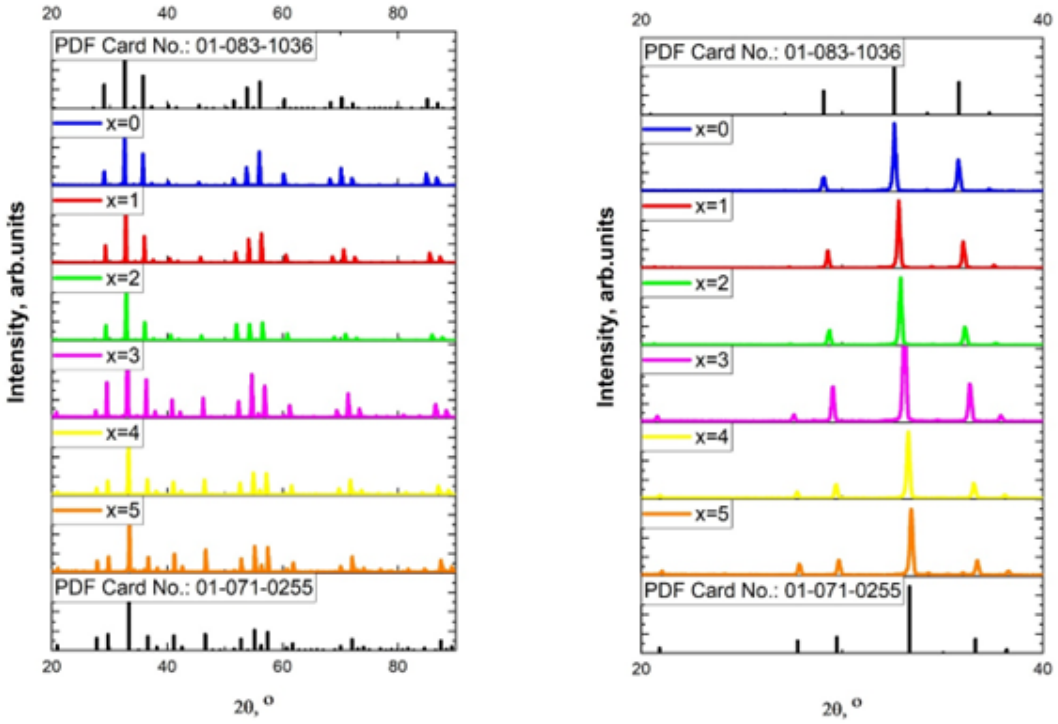

Figure 2 – XRD patterns of $Y_3Al_xGa_{5-x}O_{12}$: Ce ceramics as a function of Al/Ga ratio: (a) full 2θ range; (b) expanded view of the $2\theta = 20–40°$ region

For all investigated compositions, the diffraction patterns are fully indexed to the cubic garnet structure of the $Y_3Al_5O_{12}$ type (space group Ia^3d, PDF Card No. 01-083-1036; PDF Card No. 01-071-0255), confirming that the garnet host lattice is preserved throughout the entire Al/Ga substitution range. This result is consistent with the established solid-solution behaviour of YAG–YAGG systems reported in the literature [11].

With increasing Al^{3+} content, a systematic high-angle shift of the principal Bragg reflections is observed (Figure 2b), signalling a progressive contraction of the unit-cell parameter. This behaviour reflects the smaller ionic radius of Al^{3+} relative to Ga^{3+} in both octahedral and tetrahedral coordination environments of the garnet structure, which reduces average interatomic distances upon Al-for-Ga substitution, in quantitative agreement with published lattice-parameter data for the $Y_3Al_xGa_{5-x}O_{12}$: Ce series [11–13].

Phase analysis (Figure 3) reveals a pronounced dependence of phase purity on Al/Ga ratio. Intermediate compositions (x = 2–4) yield predominantly single-phase garnet ceramics, with secondary-phase fractions not exceeding a few per cent. At the terminal compositions, however, the phase purity deteriorates: the x = 5 (YAG: Ce) sample contains residual Al_2O_3 and $YAlO_3$ phases, while the x = 0 (YGG: Ce) endpoint exhibits Ga_2O_3 and $Y2O_3$ impurities. This behavior is consistent with the thermodynamic stability limits of the single-phase garnet field in the YAG–YGG system documented in the literature [14–16]. Notably, the compositions $Y_3Al_4GaO_{12}$: Ce and $Y_3Al_2Ga_3O_{12}$: Ce achieve garnet phase fractions exceeding 99%, identifying them as optimal Al/Ga ratios for single-phase garnet formation under the present synthesis conditions.

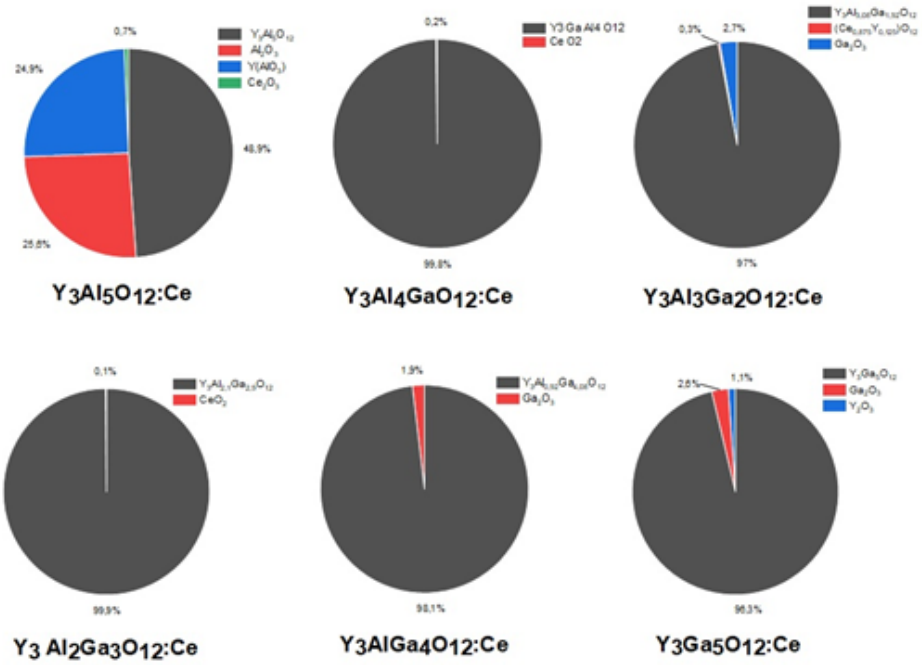

Figure 3 – Phase composition of $Y_3Al_xGa_{5-x}O_{12}$: Ce ceramics as a function of Al/Ga ratio (from Rietveld-based XRD analysis)

Photoluminescence and Excitation spectra

The excitation spectra of all investigated YAGG:Ce compositions exhibit two characteristic absorption manifolds: a near-UV band centred in the 340–370 nm range and a blue band centred in the 430–470 nm range (Figure 4). This two-band structure is the spectroscopic hallmark of the 4f → 5d electric-dipole transitions of Ce^{3+} in a garnet crystal field [17], and the observed evolution with composition is fully consistent with the crystal-field tuning model for Ce^{3+} activators in oxide hosts [18].

Progressive replacement of Al^{3+} by the larger Ga^{3+} (decreasing x) induces a systematic long-wavelength shift of the near-UV excitation band, expanding its overlap with the emission of near-UV and violet LEDs (380–410 nm). Simultaneously, the relative intensity of the blue excitation band (430–470 nm) is redistributed, which has direct implications for the coupling efficiency with InGaN blue chips [19,20]. This spectral tunability is a well-established feature of Ce^{3+}-doped mixed-garnet ceramics [19] and arises from the sensitivity of the 5d barycenter energy and crystal-field splitting to the mean metal–oxygen bond length in the garnet host.

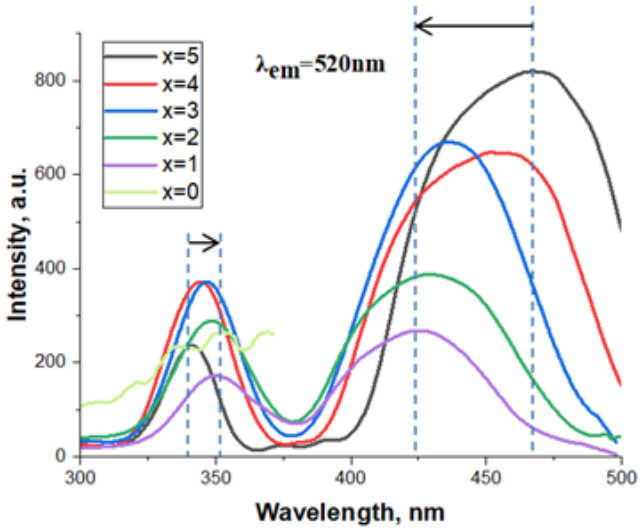

Figure 4 – Photoluminescence excitation spectra
of $Y_3Al_xGa_{5-x}O_{12}$:Ce as a function of Al^{3+}/Ga^{3+} substitution

Under 350 nm n-UV excitation (Figure 5), all compositions produce a broad 5d → 4f emission band in the visible region peaking near λ ≈ 540 nm, characteristic of Ce^{3+} in a garnet host [21]. The integrated emission intensity peaks for intermediate compositions (x = 2–4), reflecting the combined effect of optimized crystal-field strength and minimal nonradiative trap density in the near-single-phase ceramic.

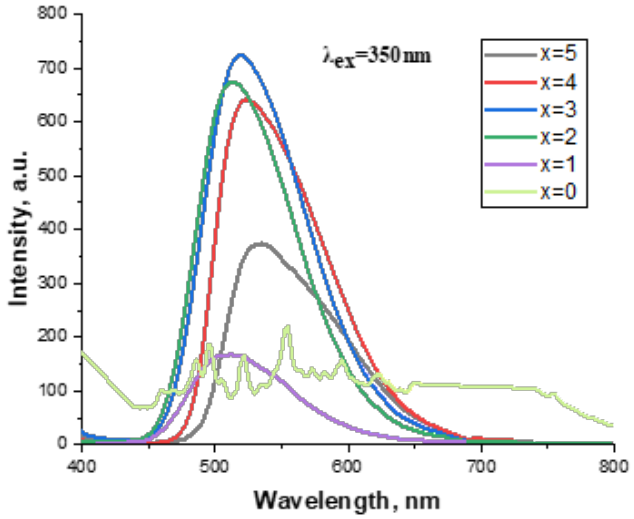

Figure 5 – Photoluminescence spectra
of $Y_3Al_xGa_{5-x}O_{12}$: Ce with different Al/Ga ratios under λ_{ex} = 350 nm excitation

Under 450 nm blue excitation (Figure 6), which replicates the operating conditions of InGaN-based white LEDs, the emission intensity exhibits a monotonic increase with decreasing x, i.e., with increasing Ga content. This trend is fully consistent with the excitation spectra: compositions with lower x develop a more intense blue absorption band, resulting in a higher photon-to-photon conversion efficiency under 450 nm pumping [22, 23].

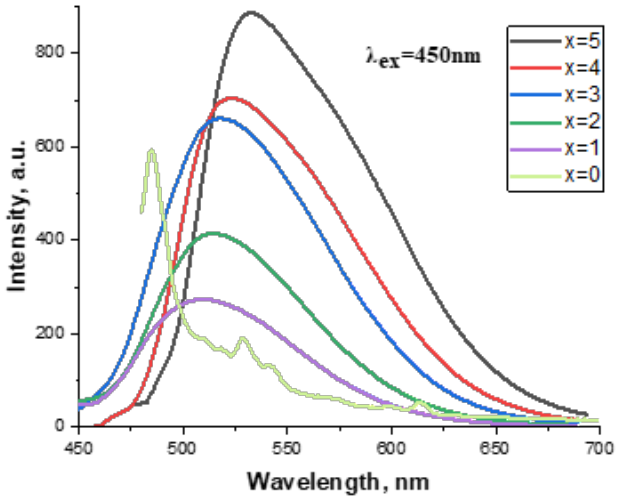

Figure 6 – Photoluminescence spectra
of $Y_3Al_xGa_{5-x}O_{12}$: Ce with different Al/Ga ratios under λ_{ex} = 450 nm excitation

The normalised PL spectra span the 480–650 nm range and are well described by the 5d → 4f allowed electric-dipole transition of Ce^{3+}. In the energy domain, the full width at half maximum (FWHM) values lie in the narrow range 0.40–0.44 eV and show only a weak dependence on excitation wavelength (Table 2). The observed variation of FWHM with Al/Ga ratio is in agreement with published data for $Y_3(Al,Ga)_5O_{12}$: Ce systems [24] and reflects the changing distribution of 5d crystal-field states upon progressive Ga-for-Al substitution in the octahedral and tetrahedral sites of the garnet lattice. The FWHM values obtained here are fully representative of Ce^{3+}-activated garnet phosphors reported to date, validating the spectroscopic methodology employed.

Table 2 – Emission bandwidth (FWHM in eV) of $Y_3Al_xGa_{5-x}O_{12}$: Ce at different excitation wavelengths

Composition	x	FWHM (ΔE), eV, λ_{ex} = 450 nm	FWHM (ΔE), eV, λ_{ex} = 350 nm
$Y_3AlGa_4O_{12}$:Ce	1	0,419	0,416
$Y_3Al_2Ga_3O_{12}$:Ce	2	0,398	0,402
$Y_3Al_3Ga_2O_{12}$:Ce	3	0,428	0,402
$Y_3Al_4GaO_{12}$:Ce	4	0,414	0,401
$Y_3Al_5O_{12}$:Ce	5	0,407	0,413

Note: Data for x = 0 (Sample 641, $Y_3Ga_5O_{12}$: Ce) are not reported. Owing to the phase impurities present in this composition, the photoluminescence emission and excitation spectra of Sample 641 exhibited negligible, non-normalizable signal, which precluded reliable determination of the emission bandwidth (FWHM) and of the CIE 1931 chromaticity coordinates/CCT.

Relative luminance

Relative luminance measurements, referenced to an SDL 4000 phosphor standard under identical geometrical and excitation conditions, provide a quantitative metric of the conversion efficiency (Figure 7). Under 340 nm n-UV excitation, the highest luminance is observed for Al-rich compositions (Al/Ga = 5/0 and 4/1), with a monotonic decrease as the Ga fraction increases. This trend reflects the reduced oscillator strength of the near-UV excitation band at high Ga content, consistent with the enhanced nonradiative relaxation associated with the lowering of the $5d^1$ level toward the conduction band minimum as documented by Dorenbos [25].

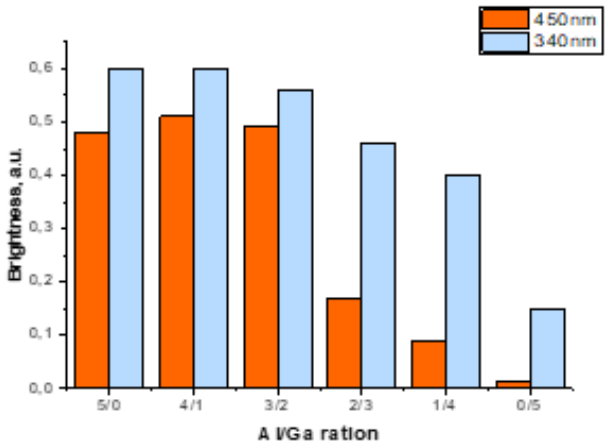

Figure 7 – Relative luminance $Y_3Al_xGa_{5-x}O_{12}$: Ce ceramic powders as a function of Al/Ga ratio under λ_{ex} = 340 nm (n-UV) and λ_{ex} = 450 nm excitation, normalised to the SDL 4000 standard

Under 450 nm blue excitation, the luminance is highest for Al-dominant compositions (Al/Ga = 5/0 to 3/2) and drops sharply as the Ga fraction exceeds 50% (Al/Ga = 2/3 to 0/5) [25]. Given that the 450–460 nm window coincides with the peak emission of standard InGaN chips, this result defines an optimal compositional range (x = 3–5) for maximizing photon conversion efficiency in conventional white LED architectures. The divergence between the luminance–composition trends under n-UV and blue excitation is an intrinsic consequence of the differential redistribution of oscillator strength between the two 4f → 5d excitation manifolds by compositional substitution, in agreement with published data for $Y_3(Al,Ga)_5O_{12}$: Ce [26].

Note that these values represent relative luminance with respect to the SDL-4000 standard rather than absolute internal/external quantum efficiency (IQE/EQE); absolute quantum efficiency, requiring integrating-sphere measurements, was not determined in this study.

Chromaticity and correlated colour temperature

CIE 1931 chromaticity coordinates were calculated from the experimental PL spectra for each composition and excitation wavelength (Figure 8a, b). The resulting colour loci and correlated colour temperatures (CCT) are compiled in Table 3.

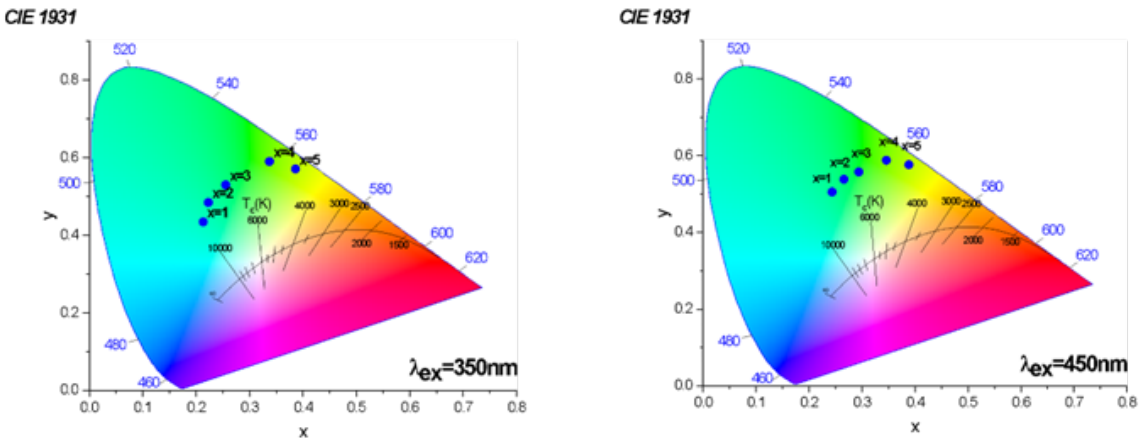

a b

Figure 8 – CIE 1931 chromaticity diagram showing the emission colour loci of $Y_3Al_xGa_{5-x}O_{12}$: Ce ceramics with different Al/Ga ratios under (a) λ = 350 nm and (b) λ = 450 nm excitation

A pronounced dependence of the CIE coordinates on excitation wavelength is observed for all compositions, which is a direct consequence of the unequal contributions of the 4f → $5d^2$ (340–360 nm) and 4f → $5d^1$ (450–470 nm) transitions to the population of the excited 5d manifold and the resulting differences in the spectral power distribution of the emission [28, 29]. Increasing Ga^{3+} content (decreasing x) shifts the chromaticity coordinates toward higher CCT values, corresponding to cooler (blue) emission, as a direct result of the reduced crystal-field splitting and the concomitant blue-shift of the Ce^{3+} emission maximum [27]. Collectively, the data in Table 3 demonstrate that the CCT is continuously tunable across a remarkably wide range–4618 to 9679 K–solely by adjusting the Al/Ga ratio and the pump wavelength, without changing the activator concentration or the matrix host cation.

Table 3 – CIE 1931 chromaticity coordinates and correlated colour temperatures (CCT) of $Y_3Al_xGa_{5-x}O_{12}$: Ce ceramics

Composition	CIE	λ_{ex} = 340 nm			λ_{ex} = 450 nm		
		x	y	CCT (K)	x	y	CCT (K)
$Y_3Al_5O_{12}$:Ce	x=5	0,3851	0,5720	4641	0,3874	0,5776	4618
$Y_3Al_4GaO_{12}$:Ce	x=4	0,3363	0,5913	5445	0,3449	0,5892	5301
$Y_3Al_3Ga_2O_{12}$:Ce	x=3	0,2544	0,5308	7247	0,2929	0,5586	6277
$Y_3Al_2Ga_3O_{12}$:Ce	x=2	0,2220	0,4855	8542	0,26484	0,5396	6952
$Y_3AlGa_4O_{12}$:Ce	x=1	0,2124	0,4354	9679	0,2425	0,5065	7722

Note: Data for x = 0 (Sample 641, $Y_3Ga_5O_{12}$: Ce) are not reported. Owing to the phase impurities present in this composition, the photoluminescence emission and excitation spectra of Sample 641 exhibited negligible, non-normalizable signal, which precluded reliable determination of the emission bandwidth (FWHM) and of the CIE 1931 chromaticity coordinates/CCT.

Diffuse reflectance spectra

Diffuse reflectance spectra recorded over the 200–600 nm range (Figure 9) are characterised by high reflectance in the long-wavelength region (λ > 500 nm), confirming the absence of strong absorption bands in the visible range–a feature expected for Ce^{3+}-activated garnet matrices [30]. Pronounced minima in the UV and near-visible regions correspond to the characteristic 4f → 5d absorption of Ce^{3+} and exhibit compositional shifts consistent with the excitation spectra (Section 3.2), corroborating the structural assignment of the spectral features.

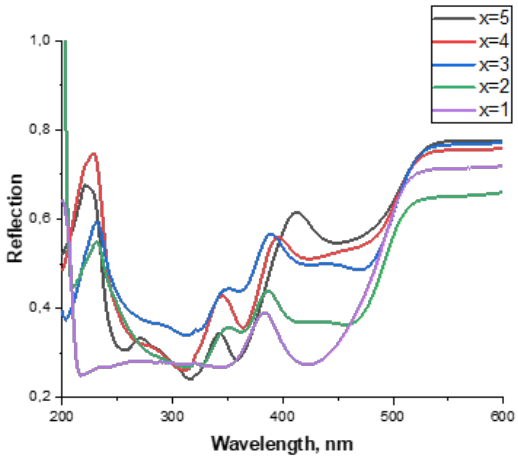

Figure 9 – Diffuse reflectance spectra of $Y_3Al_xGa_{5-x}O_{12}$:Ce ceramics as a function of Al/Ga ratio (200–600 nm)

Conclusion

Ceramic phosphors of the full $Y_3Al_xGa_{5-x}O_{12}$:Ce substitution series ($0 \leq x \leq 5$) have been synthesized for the first time by direct electron-beam radiation processing of binary oxide charge mixtures at a throughput of ≈5 g s^{-1} and a total irradiation time below 1 s per batch, without mineralizer additives or secondary energy sources. The principal findings are as follows:

◆ XRD phase analysis confirmed retention of the cubic garnet structure (space group Ia^3d) throughout the entire Al/Ga substitution range. The highest phase purity (garnet fraction > 99%) was achieved for compositions $Y_3Al_4GaO_{12}$:Ce and $Y_3Al_2Ga_3O_{12}$:Ce, while the terminal compositions (x = 0 and x = 5) showed measurable secondary-phase fractions.

◆ Systematic lattice contraction accompanies increasing Al content, consistent with the smaller ionic radius of Al^{3+} relative to Ga^{3+} in both octahedral and tetrahedral garnet sites.

◆ Compositional tuning of the Al/Ga ratio affords continuous and independent control over (i) the positions and relative intensities of the n-UV (340–370 nm) and blue (430–470 nm) excitation bands; (ii) the PL emission peak and FWHM (0.40–0.44 eV, weakly dependent on excitation wavelength); and (iii) the CIE 1931 chromaticity coordinates and CCT (4618–9679 K).

◆ Luminance analysis reveals that Al-rich compositions (x = 3–5) provide the highest photon conversion efficiency under both n-UV (340 nm) and blue (450 nm) excitation, defining the optimal compositional window for solid-state lighting applications; the non-monotonic divergence of luminance trends between n-UV and blue pumping is attributed to differential redistribution of oscillator strength between the two 4f → 5d excitation manifolds.

◆ All structural and optical properties are fully commensurate with data reported for $Y_3Al_xGa_{5-x}O_{12}$:Ce ceramics and crystals produced by conventional solid-state or solution methods, unambiguously validating the electron-beam radiation synthesis route as a viable rapid-throughput alternative for multi-component phosphor ceramics.

The established composition–property relationships provide a quantitative basis for the optimization of radiation synthesis parameters and precursor compositions in the targeted fabrication of YAGG:Ce ceramic phosphors for n-UV-pumped and blue-pumped solid-state lighting, as well as for extension of the radiation synthesis approach to other technologically relevant refractory oxide ceramics.

REFERENCES

1 Ueda, J., and Tanabe, S. Review of luminescent properties of Ce^{3+}–doped garnet phosphors: new insight into the effect of crystal and electronic structure. Optical Materials: X, 1, 100018 (2019). https://doi.org/10.1016/j.omx.2019.100018

2 Lin, Y., Bettinelli, M., Sharma, S.K., Redlich, B., Speghini, A., and Karlsson, M. Unraveling the impact of different thermal quenching routes on the luminescence efficiency of the $Y_3Al_5O_{12}:Ce^{3+}$ phosphor for white light emitting diodes. Journal of Materials Chemistry C, 8, 14015–14027 (2020). https://doi.org/10.1039/D0TC03821K

3 Du, B., Li, W., Zhang, L., Chen, P., and Lu, F. Recent advances in preparing transparent phosphor ceramics for high–index color rendering and high–power lighting. Molecules, 29 (6), 1325 (2024). https://doi.org/10.3390/molecules29061325

4 Liu, Y., Liu, S., Sun, P., et al. Transparent ceramics enabling high luminous flux and efficacy for the next–generation high–power LED light. ACS Applied Materials & Interfaces, 11 (24), 21697–21701 (2019). https://doi.org/10.1021/acsami.9b02703

5 Fang, M.–H., Bao, Z., Huang, W.–T., and Liu, R.–S. Evolutionary generation of phosphor materials and their progress in future applications for light–emitting diodes. Chemical Reviews, 122 (13), 11474–11513 (2022). https://doi.org/10.1021/acs.chemrev.1c00952

6 Tulegenova, A.T., Nogaibekova, G.Zh., Saidazimov, I.A., Vilchinskaya, S.S., and Markhabayeva, A.A. Spectral Characteristics of Photoluminescence Synthesized in the Field of Radiation YAGG Phosphors with

Different Al/Ga Ratio. Bulletin of the Karaganda University. Physics series, 4 (116), 114–122 (2024). https://doi.org/10.31489/2024PH4/114-122

7 Fu, S., Tan, J., Bai, X., Yang, S., You, L., and Du, Z. Effect of Al/Ga substitution on the structural and luminescence properties of $Y_3(Al_{1-x}Ga_x)_5O_{12}:Ce^{3+}$ phosphors. Optical Materials, 75, 573–579 (2018). https://doi.org/10.1016/j.optmat.2017.11.021

8 Khan, N.Z., Lee, H., Jo, D.Y., et al. The developments of cyan emitting phosphors to fulfill the cyan emission gap of white-LEDs. Frontiers in Chemistry, 11, 1274410 (2023). https://doi.org/10.3389/fchem.2023.1274410

9 Xia, Z., and Meijerink, A. Ce^{3+}-doped garnet phosphors: Composition modification, luminescence properties and applications. Chemical Society Reviews, 46 (1), 275–299 (2017). https://doi.org/10.1039/C6CS00551A

10 Lisitsyn, V., Tulegenova, A., Golkovski, M., Polisadova, E., Lisitsyna, L., Mussakhanov, D., and Alipysova, G. Radiation synthesis of high-temperature wide-bandgap ceramics. Micromachines, 14 (12), 2193 (2023). https://doi.org/10.3390/mi14122193

11 Sifat, R., and Grosvenor, A.P. Examination of the site preference in garnet type ($X_3A_2B_3O_{12}$; X = Y, A/B = Al, Ga, Fe) materials. Solid State Sciences, 83, 116–124 (2018). https://doi.org/10.1016/j.solidstatesciences.2018.06.013

12 Jiang, L., Zhang, X., Zhu, S., et al. Preparation and luminescence properties of $Y_{3-\gamma}Al_{5-x}Ga_xO_{12}:Ce^{3+}_{\gamma}$ phosphors. Journal of Materials Science: Materials in Electronics, 29 (11), 9350–9358 (2018). https://doi.org/10.1007/s10854-018-8930-6

13 Bartosiewicz, K., Babin, V., Kamada, K., Yoshikawa, A., Kurosawa, S., Beitlerova, A., Kucerkova, R., Nikl, M., and Zorenko, Y. Ga for Al substitution effects on the garnet phase stability and luminescence properties of $Gd_3Ga_xAl_{5-x}O_{12}$:Ce single crystals. Journal of Luminescence, 216, 116724 (2019). https://doi.org/10.1016/j.jlumin.2019.116724

14 Zhu, S., Zhang, X., Li, W., Liu, M., Cheng, L., Mi, X., and Lu, L. Phase transformation and luminescence properties of $Y_{2.94}Al_{5-x}Ga_xO_{12}:0.06Ce^{3+}$ phosphors. Ceramics International, 45 (5), 6060–6066 (2019). https://doi.org/10.1016/j.ceramint.2018.11.196

15 Kim, J.S., Kim, Y.H., Kim, H.L., et al. Tailoring trap depth and emission wavelength in $Y_3Al_{5-x}Ga_xO_{12}:Ce^{3+},V^{3+}$ persistent luminescent phosphors-in-glass films. ACS Applied Materials & Interfaces, 10 (31), 25975–25984 (2018). https://doi.org/10.1021/acsami.8b10713

16 Bolek, P., Zeler, J., Brites, C.D.S., Trojan-Piegza, J., Carlos, L.D., and Zych, E. Ga-modified YAG:Pr^{3+} dual-mode tunable luminescence thermometers. Chemical Engineering Journal, 421, 129764 (2021). https://doi.org/10.1016/j.cej.2021.129764

17 Chan, J., Cao, L., Li, W., Ma, N., Xu, Z., and Huang, X. Highly efficient broad-band green-emitting cerium(III)-activated garnet phosphor allows the fabrication of blue-chip-based warm-white LED device with a superior color rendering index. Inorganic Chemistry, 61 (18), 6953–6963 (2022). https://doi.org/10.1021/acs.inorgchem.2c00326

18 Barta, J., Pestovich, K.S., Valdez, J.A., Wiggins, B.W., Richards, C., Smith, E., Clayton, J.H., Smalley, D., and McClellan, K.J. Compositional screening of Ce-doped $(Gd,Lu,Y)_3(Al,Ga)_5O_{12}$ ceramics prepared by quenching from melt and their luminescence properties. Journal of Alloys and Compounds, 896, 161687 (2022). https://doi.org/10.1016/j.jallcom.2021.161687

19 He, C., Ji, H., Huang, Z., Wang, T., Zhang, X., Liu, Y., Fang, M., Wu, X., Zhang, J., and Min, X. Red-Shifted Emission in $Y_3MgSiAl_3O_{12}:Ce^{3+}$ Garnet Phosphor for Blue Light-Pumped White Light-Emitting Diodes. Journal of Physical Chemistry C, 122 (27), 15659–15665 (2018). https://doi.org/10.1021/acs.jpcc.8b03940

20 Qu, M.-Y., Li, T.-Q., and Liu, Q.-L. Photoluminescence Properties of Cyan-Emitting $Lu_3Ga_xAl_{5-x}O_{12}:Ce^{3+}$ Garnet Phosphors Synthesized in Nonreducing Atmosphere and at Different Temperature for High Quality w-LEDs. Materials, 15 (19), 6817 (2022). https://doi.org/10.3390/ma15196817

21 Ha, H., Yang, S., and Park, S. Photoluminescence Spectra Correlations with Structural Distortion in Eu^{3+}- and Ce^{3+}-Doped $Y_3Al_{5-2x}(Mg,Ge)_xO_{12}$ (x = 0, 1, 2) Garnet Phosphors. Materials, 17 (10), 2445 (2024). https://doi.org/10.3390/ma17102445

22 Solovjovas, A., Sidletskiy, O., Gerasymov, I., Nargelas, S., Soltanaitė, G., Podlipskas, Ž., Auffray, E., and Tamulaitis, G. Influence of gallium content on luminescence properties of Ce-doped yttrium aluminum gallium garnet scintillator. Optical Materials, 163, 117480 (2025). https://doi.org/10.1016/j.optmat.2025.117480

23 Babin, V., Buryi, M., Chlan, V., Fomichov, Y., Kamada, K., Laguta, V.V., Nikl, M., Pejchal, J., Štěpánková, H., Yoshikawa, A., Zagorodniy, Yu., and Zazubovich, S. Influence of gallium content on Ga^{3+}

position and photo- and thermally stimulated luminescence in Ce^{3+}-doped multicomponent $(Y,Lu)_3Ga_xAl_{5-x}O_{12}$ garnets. Journal of Luminescence, 200, 141–150 (2018). https://doi.org/10.1016/j.jlumin.2018.04.013

24 Zorenko, Yu., Zorenko, T., Malinowski, P., Sidletskiy, O., and Neicheva, S. Luminescent properties of $Y_3Al_{5-x}Ga_xO_{12}$:Ce crystals. Journal of Luminescence, 156, 102–107 (2014). https://doi.org/10.1016/j.jlumin.2014.07.011

25 Ma, N., Zhang, Z., Li, W., and Huang, X. Efficient blue-light-excited cyan-emitting $CaLu_2HfScAl_3O_{12}:Ce^{3+}$ phosphors for full-visible-spectrum warm-white LEDs. Journal of Luminescence, 263, 120060 (2023). https://doi.org/10.1016/j.jlumin.2023.120060

26 Dorenbos, P. 5d-level energies of Ce^{3+} and the crystalline environment. IV. Aluminates and "simple" oxides. Journal of Luminescence, 99, 283–299 (2002). https://doi.org/10.1016/S0022-2313(02)00347-2

27 Zou, J., Yang, B., Qian, X., et al. Effect of Al/Ga substitution on photoluminescence and chromatic properties of $Y_3Al_{5-x}Ga_xO_{12}:Ce^{3+}$ phosphor. Journal of Materials Science: Materials in Electronics, 27, 8074–8079 (2016). https://doi.org/10.1007/s10854-016-4806-9

28 He, X., Wang, X., Yu, H., Lei, B., Fu, Z., and Zhang, S. Effects of local structure of Ce^{3+} ions on luminescent properties of YAG:Ce phosphors. Scientific Reports, 6, 22238 (2016). https://doi.org/10.1038/srep22238

29 Khanin, V., Venevtsev, I., Chernenko, K., Pankratov, V., Klementiev, K., van Swieten, T., van Bunningen, A.J., Vrubel, I., Shendrik, R., Ronda, C., Rodnyi, P., and Meijerink, A. Exciton interaction with Ce^{3+} and Ce^{4+} ions in $(LuGd)_3(Ga,Al)_5O_{12}$ ceramics. Journal of Luminescence, 237, 118150 (2021). https://doi.org/10.1016/j.jlumin.2021.118150

30 Li, Z., Zhang, Y., Huang, Y., Wang, L., and Zheng, H. Ce^{3+} Yellow Phosphors Prepared by Different Methods. Materials, 8 (7), 4436–4447 (2015).

[1]Тулегенова А.Т.,
доцент, PhD, ORCID ID: 0000-0002-5701-6674,
e-mail: tulegenova.aida@gmail.com
[2]Лисицын В.М.,
профессор, ф.-м.ғ.д., ORCID ID: 0000-0002-2075-4796,
e-mail: lisitsyn@tpu.ru
[1]Ноғайбекова Г.Ж.,
аға оқытушы, ORCID ID: 0009-0008-8688-4279,
e-mail: nogaibekovagulnur@gmail.com
[3]Лисицына Л.А.,
профессор, ф-м.ғ.д., ORCID ID: 0000-0001-6273-6345,
e-mail: lisitsyna@mail.ru

[1]Әл-Фараби атындағы Қазақ ұлттық университеті, Алматы қ., Қазақстан
[2]Томск политехникалық университеті, Томск қ,. Ресей
[3]Томск мемелекеттік сәулет-құрылыс университеті, Томск қ,. Ресей

ЖАРЫҚДИОДТАРДА ҚОЛДАНУ ҮШІН $Y_3AL_XGA_{5-X}O_{12}$:CE ЛЮМИНОФОРЛАРЫНЫҢ ОПТИКАЛЫҚ ҚАСИЕТТЕРІНЕ AL/GA ҚАТЫНАСЫНЫҢ ӘСЕРІ

Аңдатпа

Радиациялық әдіспен алғаш рет синтезделген $Y_3Al_xGa_{5-x}O_{12}$:Ce (YAGG:Ce) керамикалық люминофорларының зерттеу нәтижелері ұсынылған. Жарық диодты жарық көздерінде қолдануға перспективалы Ce^{3+} иондарымен легирленген $Y_3Al_xGa_{5-x}O_{12}$:Ce (YAGG:Ce) гранаттары негізіндегі люминофорлардың оптикалық сипаттамаларына Al/Ga қатынасының әсері зерттелді. Белсендіруші Ce^{3+} иондарыныың концентрациясы тұрақты болған жағдайда, алюминий мен галлий мөлшері әртүрлі үлгілердің қоздыру және фотолюминесценция спектрлері талданды. Құрамның өзгеруі қоздыру және сәуле шығару жолақтарының орны мен пішінінің қайта құрылуына, фотолюминесценция жолақтарының енінің өзгеруіне, сондай-ақ

спектрдің ультракүлгін және көк аймақтарында қоздыру кезінде сәуле шығару қарқындылығының қайта бөлінуіне алып келетіні көрсетілді. Al/Ga қатынасы азайған кезде қоздыру жолағының 340-370 нм маңындағы ұзын толқынды аймаққа ығысатыны анықталды, бұл жақын ультракүлгін және күлгін диапазондағы жарықдиодтарды қолдану кезінде қоздыру тиімділігін арттырады. Алынған нәтижелер радиациялық әдісті тиімді YAGG:Ce люминофорларын синтездеу үшін қолдануға болатындығын растайды.

Түйін сөздер: люминофорлар, $Y_3Al_xGa_{5-x}O_{12}$:Ce, Al/Ga қатынасы, қозу спектрлері, фотолюминесценция, жарықдиод, ультракүлгін.

[1]Тулегенова А.Т.,
доцент, PhD, ORCID ID: 0000-0002-5701-6674,
e-mail: tulegenova.aida@gmail.com
[2]Лисицын В.М.,
профессор, д.ф-м.н., ORCID ID: 0000-0002-2075-4796
e-mail: lisitsyn@tpu.ru
[1]Ноғайбекова Г.Ж.,
ст. преподаватель, ORCID ID: 0009-0008-8688-4279,
e-mail: nogaibekovagulnur@gmail.com
[3]Лисицына Л.А.,
профессор, д.ф-м.н., ORCID ID: 0000-0001-6273-6345,
e-mail: lisitsyna@mail.ru

[1]Казахский национальный университет им. аль-Фараби, г. Алматы, Казахстан
[2]Томский политехнический университет, г. Томск, Россия
[3]Томский государственный архитектурно-строительный университет, г. Томск, Россия

ВЛИЯНИЕ СООТНОШЕНИЯ AL/GA НА ОПТИЧЕСКИЕ СВОЙСТВА ЛЮМИНОФОРОВ $Y_3AL_XGA_{5-X}O_{12}$:CE ДЛЯ СВЕТОДИОДНЫХ ПРИМЕНЕНИЙ

Аннотация

Приведены результаты исследований впервые синтезированных радиационным методом керамических люминофоров $Y_3Al_xGa_{5-x}O_{12}$:Ce (YAGG:Ce). Исследовано влияние соотношения Al/Ga на оптические характеристики люминофоров на основе Ce^{3+}–легированных гранатов $Y_3Al_xGa_{5-x}O_{12}$:Ce (YAGG:Ce), перспективных для применения в светодиодных источниках света. Проанализированы спектры возбуждения и фотолюминесценции образцов с различным содержанием алюминия и галлия при фиксированной концентрации активаторных ионов Ce^{3+}. Показано, что изменение состава приводит к перестройке положения и формы полос возбуждения и излучения, изменению ширины полосы фотолюминесценции, а также к перераспределению интенсивности излучения при возбуждении в ультрафиолетовой и синей областях спектра. Установлено, что при уменьшении отношения Al/Ga полоса возбуждения смещается в длинноволновую область вблизи 340–370 нм, что повышает эффективность возбуждения при использовании светодиодов ближнего ультрафиолетового и фиолетового диапазонов. Полученные результаты подтверждают возможность использования радиационного метода для синтеза эффективных YAGG:Ce люминофоров.

Ключевые слова: люминофоры, $Y_3Al_xGa_{5-x}O_{12}$:Ce, соотношение Al/Ga, спектры возбуждения, фотолюминесценция, светодиоды, ультрафиолет.